Journal of Power Sources 208 (2012) 144–152

Contents lists available at SciVerse ScienceDirect

Journal of Power Sources

journal homepage: www.elsevier.com/locate/jpowsour

Synthesis and characterization of sulfonated polytriazole-clay proton exchange membrane by *in situ* polymerization and click reaction for direct methanol fuel cells

Yao-Jheng Huang[a], Yun-Sheng Ye[b], Yu-Jyuan Syu[a], Bing-Joe Hwang[b], Feng-Chih Chang[a,*]

[a] Institute of Applied Chemistry, National Chiao-Tung University, Hsin-Chu, Taiwan
[b] Department of Chemical Engineering, National Taiwan University of Science and Technology, Taipei, Taiwan

ARTICLE INFO

Article history:
Received 3 November 2011
Received in revised form 1 February 2012
Accepted 2 February 2012
Available online 11 February 2012

Keywords:
Clay
In situ polymerization
Sulfonated polytriazole
Click chemistry
Proton exchange membrane

ABSTRACT

Sulfonated polytriazole-clay (SPTA-clay) nanocomposites are successfully prepared by *in situ* polymerization of SPTA using click chemistry in the presence of propargyl-functionality modified clay. The clay layers are exfoliated and well dispersed within the SPTA matrix resulting in improvements in thermal stability, mechanical strength, methanol permeability, water retention, ion channel size, and ionic cluster distribution. The SPTA-clay nanocomposite membranes with small amounts of clay in the SPTA matrices possess higher selectivity's; defined as the ratio of proton conductivity to methanol permeability, and thus have potential as proton exchange membranes (PEMs) in direct methanol fuel cells (DMFCs).

1. Introduction

Polymer electrolyte membrane fuel cells (PEMFCs) continue to receive extensive attention because they have high energy densities, high energy conversion efficiencies, are easy to refuel, and can easily be incorporated in systems design [1]. There is a wide range of potential uses for PEMFCs, including stationary, portable and automotive applications [2]. Perfluorosulfonic acid ionomers, such as Nafion, are the most studied solid polymer electrolyte membranes and are the principal polymer membranes used in direct methanol fuel cells (DMFCs), because of their good chemical and physical stabilities, high proton conductivities, and their highly interconnected ionic channels [3]. However, several drawbacks seriously limit Nafion's application including its high cost, environmental incompatibility with other materials, and especially its high methanol permeability [4]. Methanol permeating from the anode to the cathode, within the fuel cell, results in fuel loss and decreases the electrochemical performance. Thus, for methanol fuel cells, it is imperative that the solid polymer membrane used has a low methanol permeability. The development of an efficient proton exchange membrane (PEM) is one of the major challenges still holding-back the wide-scale adoption of proton exchange membrane fuel cells. In recent years, there has been much intensive effort directed toward the development of alternative lower cost PEMs with better performance [5,6]. Among the various types of PEMs trialed for fuel cell application, several nonfluorinated polymeric materials have attracted attention as alternatives to the perfluorinated polymer membranes such as Nafion® or Aciplex®, due to their advantages in terms of cost, safety of the monomers, ease of synthesis, and structural diversity [7]. A large number of PEMs have been prepared from sulfonated aromatic hydrocarbon polymers such as sulfonated poly(aryl ether sulfone) (SPES) [8], sulfonated polyimide (SPI) [9–13] and sulfonated poly(ether ether ketone) (SPEEK) [14–16]. To achieve a high proton conductivity by increasing the degree of sulfonation usually results in a high degree of water swelling that tends to degrade the membrane's mechanical properties while increasing its permeability, thereby rendering it unsuitable for use in fuel cell applications. These persistent problems demand a new method or approach – such an approach is the use of organic/inorganic hybrids nanocomposites [13,17–22].

Recently, the development of click chemistry [23] employing the highly efficient copper(I)-catalyzed Huisgen 1,3-dipolar cycloaddition [24,25] between azides and terminal alkynes has found popular appeal in the design of a variety of molecular architectures. The superior region-selectivity chemical pathway has the advantages of a short reaction time, a wide range of functionalities, a high

* Corresponding author. Tel.: +886 3 5131512; fax: +886 3 5131512.
E-mail address: changfc@mail.nctu.edu.tw (F.-C. Chang).

0378-7753/$ – see front matter © 2012 Elsevier B.V. All rights reserved.
doi:10.1016/j.jpowsour.2012.02.007

yield, and tolerance toward humidity and oxygen [25]. The method has been used to synthesize a wide variety of linear, branched and cross-linked polymers [26–28].

Polymer-clay nanocomposites have attracted great interest because of their superior engineering properties, compared to neat polymers, including good tensile strength, dimensional stability, flame-retarding properties and low permeability [29,30]. Several approaches have been used to prepare polymer-layered silicate nanocomposites, these include solution exfoliation, melt intercalation, and *in situ* polymerization intercalative [31]. However, from a morphological point of view, exfoliated polymer-clay nanocomposites rather than intercalated nanocomposites are considered as better structures for high-performance composites, because the exfoliated nanostructures have stronger synergistic interactions between the polymer matrices and the silicate layers. In our previous study [32], exfoliated polytriazole-clay (PTA-clay) nanocomposites were successfully prepared by *in situ* polymerization of PTA using click chemistry in the presence of propargyl-functionality modified clay. The resulting exfoliated PTA-clay nanocomposites, which incorporated of a small amount of clay, exhibited significant improvements in their thermal and mechanical properties.

Recently, we have reported the synthesis and characterization of sulfonated polytriazole (SPTA) membranes with different degrees of sulfonation that exhibited adequate proton conductivity and low methanol permeability in comparison with Nation 117 [33]. In addition, these SPTA membranes displayed higher proton conductivities at a lower relative humidity (RH) than Nafion 117, implying that the incorporation of N-heterocycles (triazole groups) in membranes is able to improve proton conductivity at low RH. These results indicate that the SPTA membranes have the potential to be used as PEMs in DMFC applications. The objective of this work was to prepare PEMs comprising exfoliated SPTA-clay nanocomposites using *in situ* polymerization. Based on our previous approach, we expect that the properties of the SPTA-clay nanocomposite membranes to be enhanced by the nanoscale dispersion of clay layers in the polymer matrices. The exfoliation of layered silicate nanosheets in the SPTA matrices should provide longer and more tortuous diffusive pathways for methanol transport through the membrane, while simultaneously improving its thermal and mechanical properties.

2. Experimental

2.1. Materials

Methanol (≥99.8%, Sigma–Aldrich), *N*,*N*-dimethylformamide (DMF) (TEDIA, 99.8%), HCl (37%, Sigma–Aldrich), copper(I) iodine (≥97%, Riedel-de Haën), 4,4′-diazido-2,2′-stilbenedisulfonic acid, disodium salt hydrate (DADSDB) (97.0%, Sigma–Aldrich) and sodium montmorillonite (Na^+-MMT, with 1.45 mequiv. g cationic exchange capacity, Nanocor Co) were used as received. 4-(Prop-2-ynyloxy)benzenaminium (PBA) and 4,4′-(propane-2,2-diyl)bis((prop-2-ynyloxy)benzene) (PBPB) were synthesized as described in our previous paper [32,34].

2.2. Modification of clay

The propargyl-functionality modified clay was prepared through cationic exchange between Na^+-MMT and the clay-modifying agent (PBA) in an aqueous solution. Na^+-MMT was dispersed in deionized water at 60 °C, while a separate solution of PBA in deionized water was heated with mixing at 60 °C for 24 h. The propargyl-functionality modified clay was recovered by filtration, followed by repeated washing of the filter cake with deionized water to remove the excess ions. The final product was dried in a vacuum oven at room temperature for 24 h.

2.3. Preparation of the SPTA and SPTA-clay nanocomposites

The propargyl-functionality modified clay (containing 1, 3, or 5 wt.% of the monomer) was mixed with monomers (DADSDB and PBPB) and DMF in a three-necked flask and heated to 70 °C for 30 min. CuI (5.0 mol%) was added and the mixture stirred for 24 h. Copper salts were filtered and the SPTA-clay nanocomposites were obtained by precipitation in methanol, prior to filtration and overnight Soxhlet extraction with methanol. The polymer was dried at 60 °C *in vacuo* for at least 24 h. Sulfonated polytriazole (SPTA) was synthesized as described previously [33].

2.4. Film casting and membrane acidification

The SPTA and SPTA-clay membranes were prepared through solution-casting and evaporation. Polymer powders were dissolved in DMF at room temperature as a 10 wt.% solution and cast onto a glass plate prior to heating at 60 °C for 48 h. Each membrane was soaked in methanol at room temperature to remove any residual DMF, and then peeled from the glass plate during immersion in deionized water. The membranes were obtained in 'acidic form' by immersing them in 1 M HCl solution for 24 h and then washing them with deionized water until the pH was in the range 6–7.

2.5. Immersion and freeze-drying process

Freeze-drying was used to study the morphology of the SPTA-clay nanocomposites after immersion in deionized water. Firstly, the membranes were immersed in deionized water for 1 day and then immediately frozen by immersing them for 10 min in liquid nitrogen at −195 °C. Finally, the icy layer that covered the polymer surface was progressively removed by sublimation at low temperature (−170 °C), for 1 h; during which time the pressure and temperature were increased to 1.0×10^{-4} Torr and to −30 °C, respectively, to remove the residual water content.

2.6. Membrane characterizations

NMR spectra were recorded at 25 °C on an INOVA 500 MHz NMR spectrometer. The thermal degradation behavior of the membrane was measured using a Q50 thermogravimetric analyzer (TGA). The sample is heated at 120 °C for 30 min to ensure the elimination of residual water and then cooled to 40 °C. The second procedure is heating from 40 to 800 °C at a heating rate of 20 °C min^{-1} and all the procedures are under nitrogen atmosphere. Molecular weights and molecular weight distributions were determined by gel permeation chromatography (GPC) using a Waters 510 HPLC equipped with a 410 differential refractometer, a refractive index (UV) detector, and three ultrastyragel columns (100, 500, and 103 Å), connected in series, in order of increasing pore size. The tensile strength properties were measured according to ASTM 638 on a Shimadzu AG-50kNE universal tester at a crosshead speed of 1 mm per minute. The membrane morphologies were characterized using a JEOL TEM-1200EX-II instrument operated at 120 kV. To stain the hydrophilic domains, the membranes were converted into their Pb^{2+} forms by immersing in $Pb(AC)_2$ (Lead acetate, 1 N) solution overnight and then rinsing with water. Membranes were dried under vacuum at 80 °C for 12 h and then sectioned into 50 nm slices using an ultramicrotome. The slices were picked up with 200 mesh copper grids for TEM observation. Wide-angle X-ray diffraction (WAXD) spectra were recorded on powdered samples using a Rigaku D/max-2500 type X-ray diffraction instrument. The ion exchange capacity (IEC) of each sample was determined by

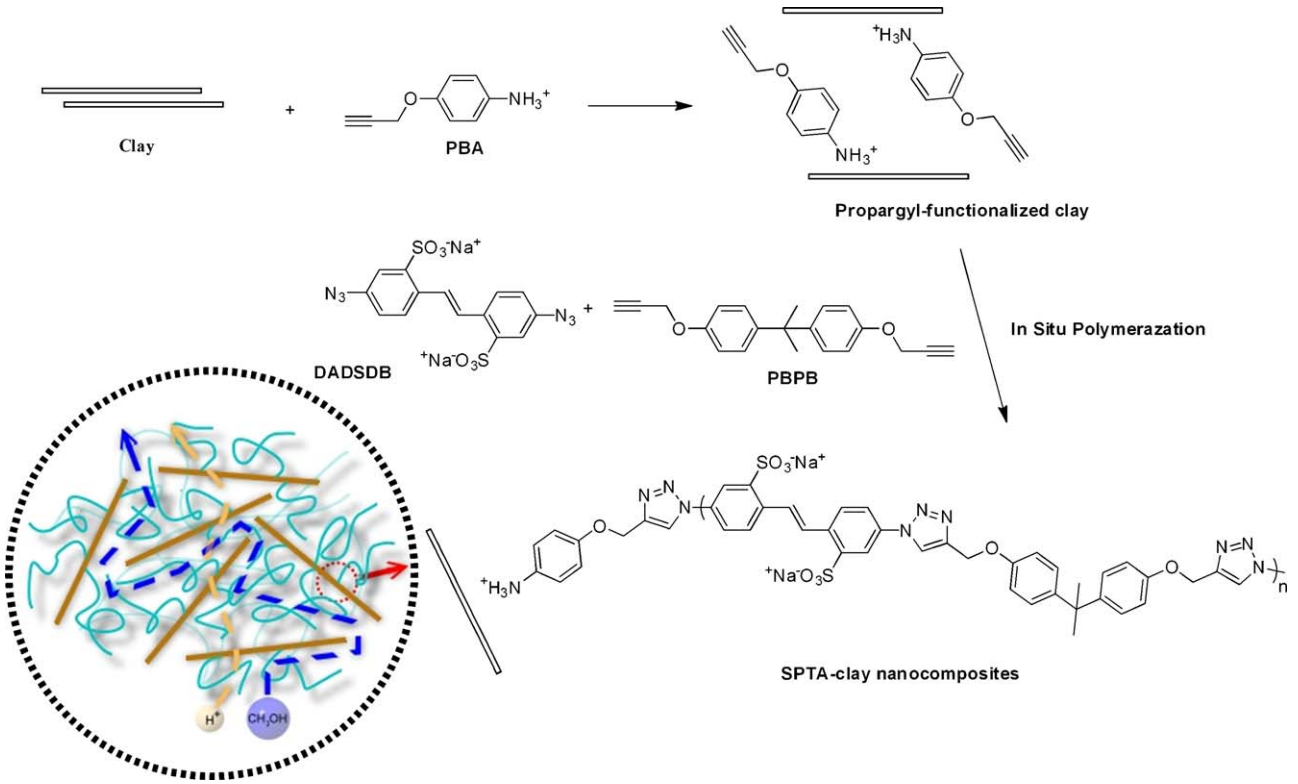

Scheme 1. Click reaction between propargyl-functionalized clay and PBPB and DADSDB by *in situ* polymerization.

the back-titration method. The membrane in the acid form was immersed in 1 M NaCl solution to convert the sulfonic acid into sodium form and the released H^+ was back titrated with a 0.01 N NaOH solution using phenolphthalein as indicator. The IEC is the equivalents per gram of dry polymer [35].

The water uptake (WU; %) was calculated using Eq. (1) [15]:

$$\mathrm{WU}\,(\%)\frac{W_{\mathrm{wet}}-W_{\mathrm{dry}}}{W_{\mathrm{dry}}}\times 100\% \tag{1}$$

The dried SPTA membranes were immersed in deionized water at room temperature for 24 h, blotted with filter paper to remove any excess surface water, and immediately weighed to obtain their wet masses (W_s). The membranes were then dried at 120 °C for 24 h to get their dry weights (W_d).

The proton conductivity of the membrane was determined with an ac electrochemical impedance analyzer (PGSTAT 30); the ac frequency being scanned from 100 kHz to 10 Hz at a voltage amplitude of 10 mV. The membrane (1 cm in diameter) was sandwiched between two smooth stainless steel disk electrodes in a cylindrical PTFE holder. The proton conductivity was calculated according to Eq. (2) [15]:

$$\sigma=\frac{L}{RA} \tag{2}$$

where σ is the proton conductivity (in $\mathrm{S\,cm^{-1}}$), L is the distance between the electrodes, A is the membrane section area (in $\mathrm{cm^2}$), and R is the impedance of the membrane (in ohm).

Water desorption measurements were performed using a TGA Q50 to determine weight changes over time at 60 °C. The water diffusion coefficient was calculated according to Eq. (3) [36]:

$$\frac{M_t}{M_\infty}=4\left(\frac{Dt}{\pi L^2}\right)^{1/2} \tag{3}$$

where D is the water diffusion coefficient, M_t/M_∞ represents the water desorption, and L is the membrane's thickness.

The methanol diffusion coefficient of the membrane was measured using a two-chamber liquid permeability cell. The description of this cell has been described in detail previously [37]. The methanol concentrations in the water cell were determined periodically using a GC-8A gas chromatograph (SHTMADU, Tokyo, Japan). The methanol permeability was calculated using Eq. (4) [15]:

$$C_B(t)=\frac{A}{V_B}\frac{P}{L}C_A(t-t_0) \tag{4}$$

where L is the membrane thickness, A is the membrane area, C_A and C_B are the methanol concentrations in the methanol and water chambers, respectively, and P is the methanol diffusion coefficient.

3. Results and discussion

3.1. Syntheses and characterizations of SPTA-clay nanocomposites

In our previous study, we successfully prepared propargyl-functionalized modified clay wherein the azide containing monomer could be attached onto the clay layer through click chemistry [32]. Propargyl-functionalized modified clay was mixed with DADSDB and PBPB monomers and polymerized to produce a series of SPTA-clay composites (Scheme 1). Table 1 shows the molecular weights (M_w) and the polydispersity index (PDIs) of the SPTA and

Table 1
Polymerization of SPTA in the presence of: 0, 1, 3, and 5 wt.% clay.

Sample	Clay loading (wt.%)[a]	M_w ($\times 10^6$)	M_w/M_n	Thickness (μm)
SPTA	0	6.58	3.30	145
SPTA 1	1	5.88	3.21	101
SPTA 3	3	5.75	3.63	112
SPTA 5	5	5.15	3.74	98

[a] Determined by the initial clay loading and mass of monomer used.

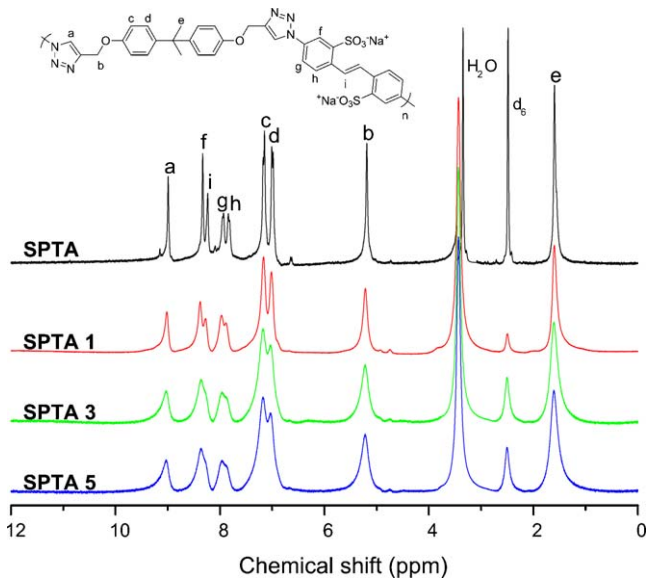

Fig. 1. ^{1}H NMR spectra of SPTA and SPTA-clay nanocomposites.

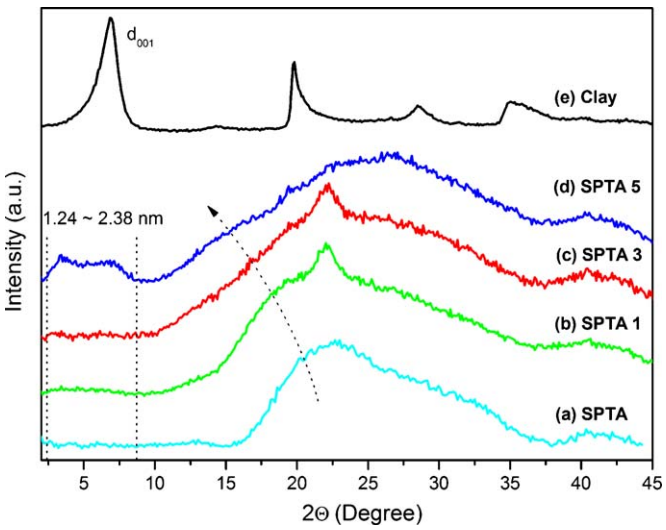

Fig. 2. Wide-angle X-ray diffraction patterns of neat SPTA and SPTA-clay nanocomposites with different clay contents.

its composites. The high efficiency of the click polymerization was clearly demonstrated by ^{1}H NMR analysis (Fig. 1). The formation of the triazole unit is revealed by the appearance of a peak at 9.00 (a) ppm, and the signal shifts of the methylene protons adjacent to the alkyne from 4.71 ppm to 5.20 (b) ppm. The integral intensity ratios of the peaks at 7.81 (h) and 7.94 (g) ppm with respect to those at 7.01 (d) and 7.14 (c) ppm are close to 1.0:2.0, implying that the SPTA and its nanocomposites were synthesized successfully. Moreover, the broad signals observed in the spectrum of polymers reveal that high molar mass SPTA and its nanocomposites were obtained. These results are in good agreement with our previous study [32].

3.2. Morphology of the SPTA-clay nanocomposites

3.2.1. Clay dispersion in SPTA-clay nanocomposites

A fully exfoliated nanocomposite possesses a higher tortuosity factor and a greater aspect ratio in comparison to partially intercalated nanocomposites and thus serves as a more effective membrane barrier for gas or methanol [30]. Fig. 2 shows the XRD patterns of neat SPTA (a), and a series of SPTA-clay nanocomposites with different clay contents (b–d, comprising 1, 3 and 5% clay, respectively) and the pristine MMT (e). For the SPTA 1 and SPTA 3 nanocomposites, the d_{001} peak of the pristine MMT completely disappeared, indicating the formation of an exfoliation structure in the nanocomposites. SPTA with 5% clay has a broad peak with d-spacing from 1.24 to 2.38 nm, indicating that both exfoliated and intercalated structures are present. Moreover, the amorphous peak of the neat SPTA (near $2\theta = 22.5^{\circ}$) shifts slightly lower with increasing clay contents in SPTA matrix – because the presence of clay plates in the SPTA matrix tends to expand the intermolecular main chain spacing [38,39].

To show the dispersion of clay in the polymer matrix, TEM micrographs, where the dark lines represent the clay layers and the bright area denotes the SPTA matrix, are shown in Fig. 3. The XRD pattern of SPTA 1 and SPTA 3 shows only the broad peak of the SPTA matrix, while TEM micrographs [Fig. 3(a) and (b)] reveal fully exfoliated clay layers consisting of evenly dispersed parallel layers. When the clay loading content reaches 5 wt.% a slight degree of aggregation, in the form of intercalated stacks, is observed, see Fig. 3(c). This image also clearly reveals that exfoliated and intercalated structures coexist in the SPTA 5 composite. This result supports the XRD analysis result with respect to the formation of exfoliated nanocomposites.

3.2.2. Effect of clay loading on ionic channel size of SPTA-clay nanocomposites

It is well known that size of the ionic channels directly affects the ionic, water and methanol permeabilities of the membrane. Although XRD has been widely used to estimate the ionic channel size in sulfonated polymers, it may not give an accurate representation of the membrane in use because the membrane when examined by XRD is in a non-hydrated state. In order to avoid the unstable water molecule that evaporation during measurement, we

Fig. 3. TEM images of (a) SPTA 1 (b) SPTA 3 and (c) SPTA 5 nanocomposite membranes.

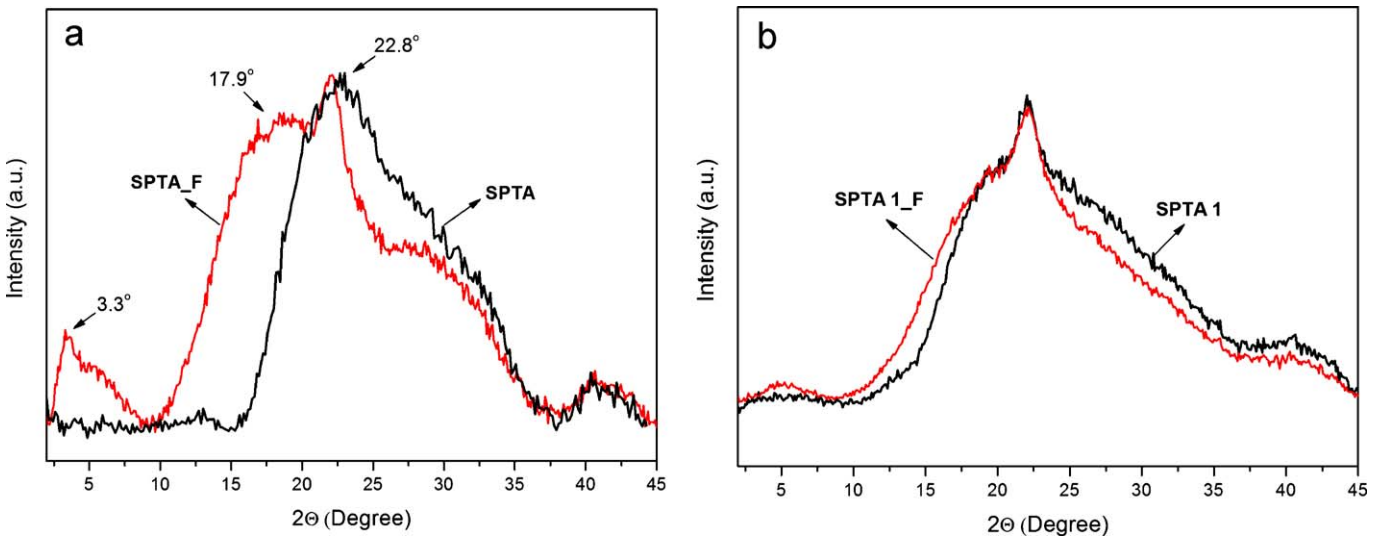

Fig. 4. Wide-angle X-ray diffraction patterns of: (a) neat SPTA and (b) SPTA 1 hybrid membranes after freeze-drying (SPTA_F and SPTA 1_F) compared to the dry state.

used the freeze-drying process (in liquid nitrogen) [33] to preserve the morphology of the hydrated state of SPTA membranes.

Fig. 4 shows the XRD patterns of (a) neat SPTA and (b) SPTA 1 after freeze-drying compared to their dry states. In Fig. 4(a), the amorphous peak of the pure SPTA ($2\theta = 22.8^\circ$) shifts to a lower value ($2\theta = 17.9^\circ$) and a new broad amorphous peak at $2\theta = 3.3^\circ$ appears in response to the freeze-drying process, indicating the larger ionic channel sizes in the water swollen membrane. In contrast, the amorphous maximum for the SPTA 1 composites remains essentially the same before and after freeze-drying [Fig. 4(b)], implying that the changes of ionic channel sizes are not obviously by introducing clay in the SPTA 1 membrane. Therefore, we suspected that the dimensions of the ionic channel are restricted by introducing clay in the SPTA membrane – evidence for changes in ionic channel size of the composite membranes (fabricated by freeze-drying) can be found in the XRD patterns (Fig. 5). Comparing the XRD patterns of pristine SPTA with the hybrid membranes, it is apparent that the cross-sectional size of the ion channels is reduced by introducing clay. This observed reduction is probably

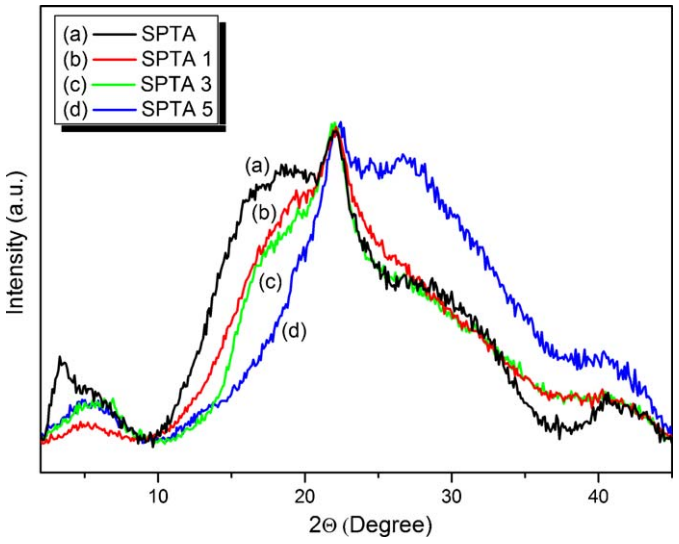

Fig. 5. Wide-angle X-ray diffraction patterns of neat SPTA and SPTA-clay nanocomposite membranes, with different clay contents, after freeze-drying.

responsible for the reduced methanol crossover rate through the electrolyte membrane.

The electrochemical properties of PEMs are closely related to their microstructures, especially the spatial distribution of their ionic sites [15,40,41]. The two images in Fig. 6 show TEM micrographs of (a) SPTA and (b) SPTA 1 membranes where the darker regions represent localized hydrophilic ionic clusters and the lighter parts represent hydrophobic moieties. As we know, the TEM images are not fully representative of the distribution of the ionic clusters in the hydrated membrane in hydrogen form because (i) the exchange of lead ions for protons could alter the cluster morphology and (ii) the membrane dehydration under vacuum at 80 °C could alter the cluster connectivity besides reducing their size. However, it will not greatly influence the observation of ionic clusters for us to compare SPTA with SPTA-clay membranes. The pure SPTA membrane possesses non-uniform ionic clusters from a few nm to 80 nm. The SPTA 1 hybrid, however, exhibits well-distributed ionic clusters in the range between 20 and 30 nm. The better ionic cluster distribution within SPTA 1 compared to pure SPTA can be attributed to the clay layers promoting size-contraction of the ion clusters, thus preventing the hydrophilic sulfonic groups of the pure SPTA from aggregating into larger ionic clusters; the overall effect being improved proton conductivity and reduced methanol permeability.

3.3. Ionic exchange capacity (IEC) and water behaviors

Owing to the small amount of clay loading, the IEC values of SPTA and SPTA-clay hybrid membranes ranged from 2.31 to 2.43 mequiv. g^{-1} shown in Table 2 indicate that the change are not obviously. The decrease in IEC value with the increase in clay loading content is due to the increase in the overall heterogeneous material (clay) content.

Water plays an important role in PEMs, directly affecting proton transport. It is imperative to enhance the water uptake (WU) of the membrane, especially at low RH and high temperature, to preserve its proton conductivity. The WUs of SPTA and SPTA-clay hybrid membranes were evaluated at 30 °C, the resulting data are presented in Table 2. It is well known that the monovalent ions located between the clay layers allow the absorption of polar solvents such as water [42–44]. The introduced clay causes a significant increasing of membrane swelling; however, when the clay loading increases from 1 to 5 wt.%, the WU at 30 °C decreases progres-

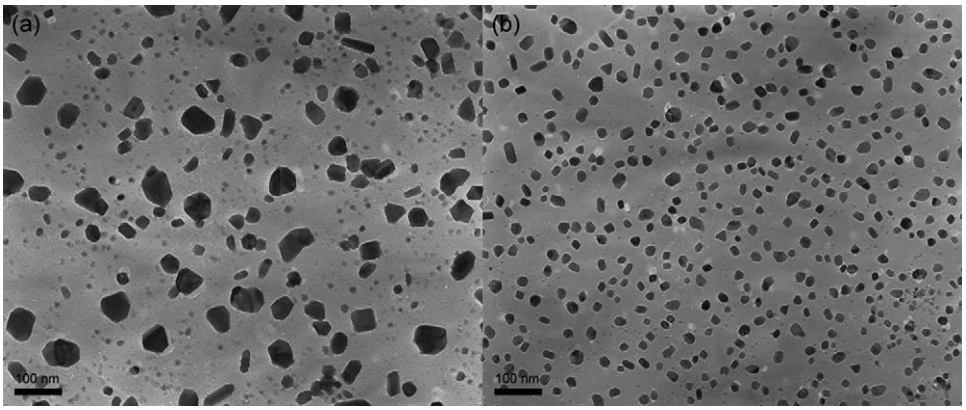

Fig. 6. TEM micrographs of: (a) SPTA and (b) SPTA 1 membranes.

Table 2
Properties of SPTA and SPTA-clay nanocomposite membranes.

Code	IEC (mequiv. g^{-1})[a]	Water uptake (wt.%)[b]	Proton conductivity σ (S cm^{-1})[c]		Methanol permeability P ($\times 10^{-6}$ cm^2 s^{-1})[b]	Selectivity $\Phi \times 10^5$ (S cm^{-3} s)
			σ_{30} at 30 °C	σ_{80} at 80 °C		Φ_{30} (σ_{30}/P)
SPTA	2.43	35.7	0.045	0.107	0.45	1.00
SPTA 1	2.41	43.8	0.044	0.122	0.21	2.10
SPTA 3	2.36	39.9	0.034	0.115	0.16	2.13
SPTA 5	2.31	38.7	0.023	0.097	0.24	0.96
Nafion 117	0.78	35.6	0.093	0.139	1.31	0.71

[a] Ion exchange capacity measured with titration.
[b] Measured at 30 °C.
[c] Measured at 90 RH.

sively from 43.8 to 38.7% due to silicate-layer aggregation resulting from the higher loading as shown in TEM images (Section 3.2.1). Additional information concerning the water behavior of SPTA and hybrid membranes can be gained by examining its relation to RH variation. Examining the WU as a function of RH at 60 °C [Fig. 7(a)], it can be seen that the reduction of the WU is less dramatic with the addition of clay in the SPTA matrix, which also implies that the anisotropic clay layers display a higher propensity for retaining water.

The water retention and diffusion properties of PEMs have significant implications for proton conductivity, especially at high temperatures and low RHs which is very important in view of their intended application in PEMFC. The water desorption curves of SPTA and SPTA-clay membranes are shown in Fig. 7(b). The exfoliated nanocomposite membrane (SPTA 1) displays a significant improvement in its water retention. The anisotropic clay layers create tortuous paths and therefore reduce the rate of transport through the hybrid membrane [45,46]. These findings are in good agreement with the relationship between the WU and the RH data mentioned above, which may be summarized by noting that the water retention of the hybrid membranes at relatively high temperatures is improved by the introduction of clay.

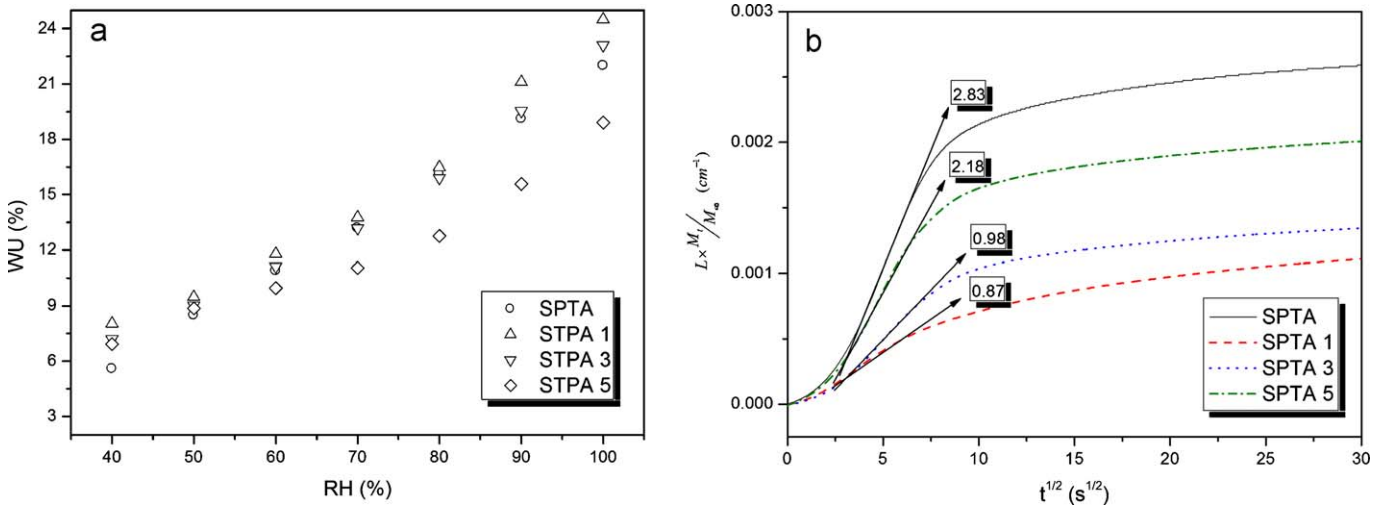

Fig. 7. (a) The WU of SPTA and SPTA-clay nanocomposite membranes at 60 °C as a function of RH. (b) The water desorption of SPTA and SPTA-clay nanocomposite membranes. The numbers in the boxes correspond to the water diffusion coefficients ($\times 10^{-5}$ cm^{-2} s^{-1}).

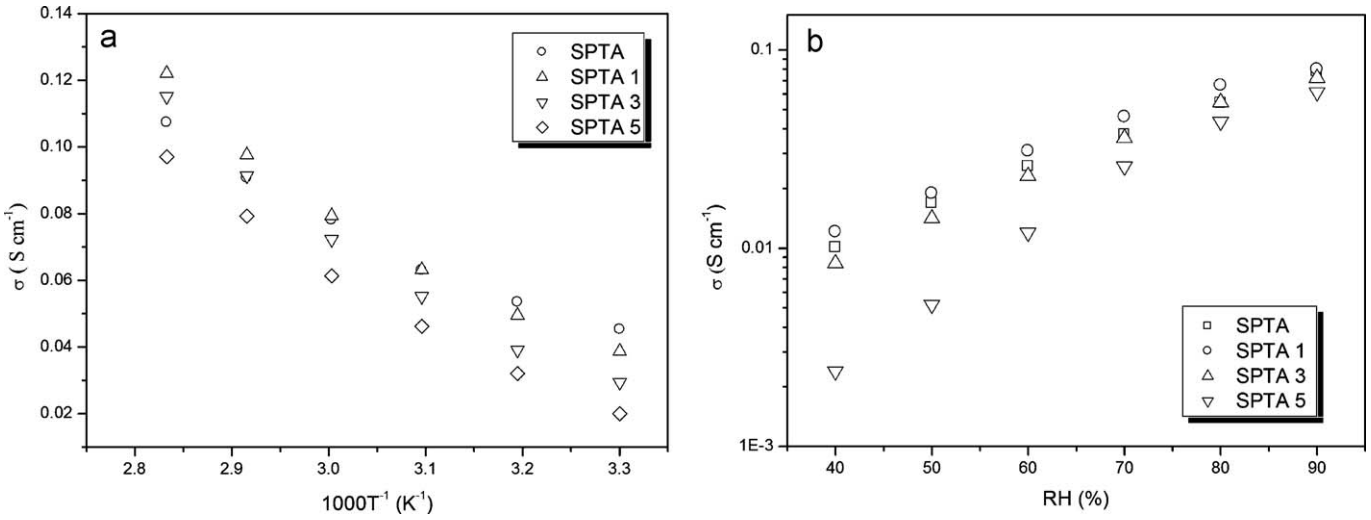

Fig. 8. Proton conductivities of SPTA and SPTA-clay nanocomposite membranes plotted as function of: (a) inverse temperature with 90% RH and (b) RH at 60 °C.

3.4. Proton conductivity and methanol permeability

The proton conductivities of the SPTA and SPTA hybrid membranes at different temperatures (30–80 °C) with 90% RH are shown in Fig. 8(a) and their relative values are listed in Table 2. Although the WU of the hybrid membrane is increased with the addition of clay; the proton conductivity decreases incrementally with clay additions at 30 °C. This can be attributed to the increase in proton transport pathways together with the decrease in the size of the ionic channels, eventually resulting in a reduction of the proton transfer ability of the membranes [47–50]. The performance of the exfoliated membranes (SPTA 1 and SPTA 3) becomes higher than that of pure SPTA. This is presumably due to the well-dispersed clay and ionic clusters (Section 3.2.2) that promote proton transport and water retention. However, the proton conductivity of the hybrid membrane gradually declines at 80 °C when the clay loading content is increased to 5 wt.%. Thus, aggregation of clay at higher clay contents, shown in the TEM images (Section 3.2.1), retards proton transportation from the anode to the cathode as mentioned previously. The proton conductivity of the SPTA-clay membranes as a function of the RH at 60 °C is shown in Fig. 8(b). The proton conductivity decreases significantly as the RH decreases, a common phenomenon that has been observed for many other sulfonated polymer membranes. It should be noted that the proton conductivity is slightly increased by the incorporation of even a small amount of clay (1 wt.%) when in the humidity range of 40–90% RH. This result indicates that the exfoliated clay nanocomposites membrane has higher water retention and higher proton conductivity at low RH.

Methanol permeability is an important membrane property in DMFC applications as the crossover of methanol from the anode to the cathode will lead to a lower cell voltage and a lower fuel efficiency. The methanol diffusion coefficients of the SPTA, SPTA hybrid membranes and Nafion 117 at 30 °C were measured and the results are presented in Fig. 9 and Table 2. The methanol diffusion coefficient decreases with increasing clay loading up to 3 wt.% but increases at 5 wt.%. Two main factors compete to determine the methanol permeability of the membranes, (i) the cross-sectional size, and (ii) the diffusive pathway of the ionic channels in the membrane. It is generally accepted that methanol permeability strongly depends on the cross-sectional size of the ionic channels [50]. As mentioned above, the cross-sectional size of the ionic channels is reduced by introducing of clay into the membrane (Section 3.2.2). It is therefore expected that the methanol permeability should be decreased by reducing the size of the ionic channels. However, SPTA 3 shows the lowest methanol permeability (0.16×10^{-6} cm^2 s^{-1}) compared to the neat SPTA (0.45×10^{-6} cm^2 s^{-1}). The exfoliated clay structure is able to generate more tortuous and longer diffusive path than the intercalated clay structure [18,35,51]. The lower methanol permeability of the SPTA-clay nanocomposite membranes compared to Nafion 117 and SPTA membranes is one of the significant advantages of DMFC systems.

Membranes suitable for use as PEMs in DMFCs require high proton conductivities and low methanol permeabilities; thus, the ratio of the proton conductivity to the methanol permeability, Φ, is an effective parameter for evaluating the membrane's performance in DMFCs. Table 2 shows the effective selectivity at 30 °C for SPTA and SPTA hybrid membranes. All the hybrid membranes exhibit higher selectivity compared to Nafion 117. The incorporation of 3 wt.% clay into the SPTA membrane results in the best selectivity. The slight decrease in ionic conductivity for the clay based nanocomposites is able to be compensated for by the large decrease in methanol permeability.

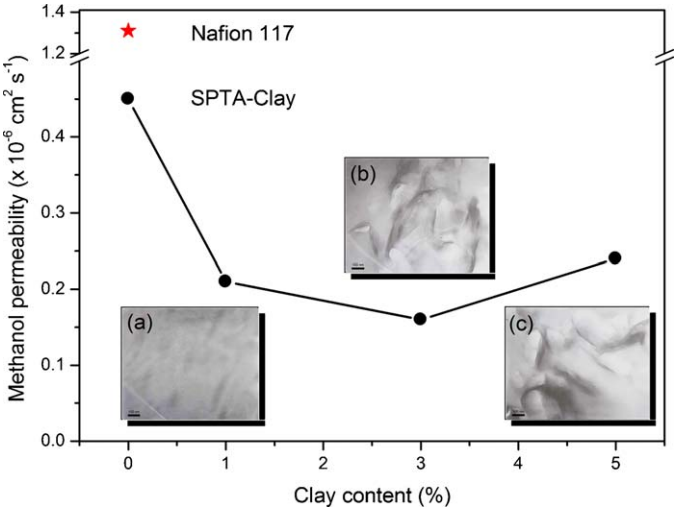

Fig. 9. Methanol permeabilities of SPTA and SPTA-clay nanocomposite membranes as a function of clay content. Insets are bright-field TEM images corresponding to the three nanocomposite membranes.

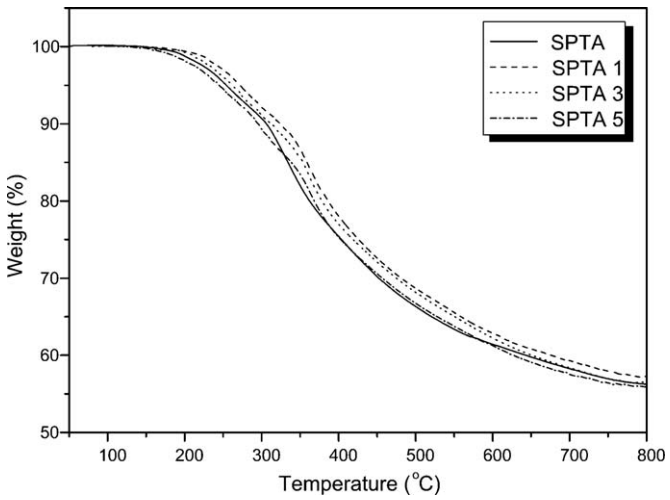

Fig. 10. TGA curves of SPTA and SPTA-clay nanocomposite membranes.

Table 3
Thermal and mechanical properties of SPTA and SPTA-clay nanocomposite membranes.

Code	T_{d5}	Tensile strength (MPa)[a]	Tensile modulus (GPa)[a]	Elongation at break (%)[a]
SPTA	254	24.7	4.38	7.05
SPTA 1	273	29.8	4.52	9.46
SPTA 3	260	31.4	4.68	9.35
SPTA 5	242	25.1	4.53	8.11

[a] Measured in the hydrated state.

3.5. Thermal and mechanical properties

Fig. 10 shows TGA thermograms and temperatures for thermal weight losses (T_{d5}) – these are also summarized, together with the membranes' mechanical properties, in Table 3. SPTA 1 and SPTA 3 membranes exhibit a higher T_{d5} than neat SPTA, due to the formation of a clay char that acts as a mass transport barrier and an isolator between the bulk polymer and the surface where the combustion takes place [52–54]. It is noteworthy that the T_{d5} of the hybrid membrane decreases with an increase in the clay loading content. This is probably because greater aggregation, i.e. with the higher clay content, leads to lower organic–inorganic interactions and thus the aggregated clay can be considered as a defect rather than as a helpful filler. The mechanical properties of all the SPTA-clay membranes are better than the pure SPTA membrane. Clay contents, of 1 and 3 wt.%, result in better mechanical properties, while the 5 wt.% clay content results in poorer mechanical properties.

4. Conclusions

We have successfully synthesized SPTA-clay nanocomposites by *in situ* polymerization using a click chemistry process. The hybrid membranes (SPTA 1 and SPTA 3) showed improved properties in terms of mechanical strength, thermal stability, methanol permeability, water retention, ion channel size, and ion cluster distribution; due to the exfoliated clay layers in the SPTA matrix. Although the proton conductivities of the SPTA-clay nanocomposite membranes decrease slightly, the effective selectivity (ratio of conductivity over methanol permeability) of nanocomposite membranes (SPTA 1 and SPTA 3) are still higher than those of neat SPTA. The substantial reduction in methanol permeability of the clay based nanocomposite membranes is able to compensate for the slight decrease in ionic conductivity. Excessive clay contents tend to lead to aggregate formation in the form of intercalation and thus reduce the exfoliated material content within the SPTA matrix; thereby, degrading the performance of the membranes. The SPTA-clay nanocomposite membrane with a small amount of clay incorporated in its SPTA matrix possesses improved physical and chemical properties and thus offers promise for use in PEMs in DMFCs.

Acknowledgement

This study was support financially by the National Science Council, Taiwan (Contract No. NSC-98-2218-E-009-001).

References

[1] S. Srinivasan, R. Mosdale, P. Stevens, C. Yang, Annu. Rev. Energy Environ. 24 (1999) 281–328.
[2] B.C.H. Steele, A. Heinzel, Nature 414 (2001) 345–352.
[3] K.A. Mauritz, R.B. Moore, Chem. Rev. 104 (2004) 4535–4586.
[4] M.A. Hickner, H. Ghassemi, Y.S. Kim, B.R. Einsla, J.E. McGrath, Chem. Rev. 104 (2004) 4587–4612.
[5] S.J. Peighambardoust, S. Rowshanzamir, M. Amjadi, Int. J. Hydrogen Energy 35 (2010) 9349–9384.
[6] R. Devanathan, Energy Environ. Sci. 1 (2008) 101–119.
[7] C.Y. Wang, Chem. Rev. 104 (2004) 4727–4766.
[8] K. Miyatake, Y. Chikashige, E. Higuchi, M. Watanabe, J. Am. Chem. Soc. 129 (2007) 3879–3887.
[9] N. Asano, M. Aoki, S. Suzuki, K. Miyatake, H. Uchida, M. Watanabe, J. Am. Chem. Soc. 128 (2006) 1762–1769.
[10] Y.S. Ye, Y.J. Huang, C.C. Cheng, F.C. Chang, Chem. Commun. 46 (2010) 7554–7556.
[11] C.Y. Tseng, Y.S. Ye, J. Joseph, K.Y. Kao, J. Rick, S.L. Huang, B.J. Hwang, J. Power Sources 196 (2011) 3470–3478.
[12] L. Akbarian-Feizi, S. Mehdipour-Ataei, H. Yeganeh, Int. J. Hydrogen Energy 35 (2010) 9385–9397.
[13] C.Y. Tseng, Y.S. Ye, M.Y. Cheng, K.Y. Kao, W.C. Shen, J. Rick, J.C. Chen, B.J. Hwang, Adv. Energy Mater. 1 (2011) 1220–1224.
[14] S. Zhong, X. Cui, H. Cai, T. Fu, C. Zhao, H. Na, J. Power Sources 164 (2007) 65–72.
[15] Y.S. Ye, Y.C. Yen, C.C. Cheng, W.Y. Chen, L.T. Tsai, F.C. Chang, Polymer 50 (2009) 3196–3203.
[16] M. Han, G. Zhang, M. Li, S. Wang, Y. Zhang, H. Li, C.M. Lew, H. Na, Int. J. Hydrogen Energy 36 (2011) 2197–2206.
[17] T.J. Pinnavaia, Science 220 (1983) 365–371.
[18] Y.S. Choi, T.K. Kim, E.A. Kim, S.H. Joo, C. Pak, Y.H. Lee, H. Chang, D. Seung, Adv. Mater. 20 (2008) 2341–2344.
[19] R. Kannan, B.A. Kakade, V.K. Pillai, Angew. Chem. Int. Ed. 47 (2008) 2653–2656.
[20] D. Xing, G. He, Z. Hou, P. Ming, S. Song, Int. J. Hydrogen Energy 36 (2011) 2177–2183.
[21] Y.S. Ye, C.Y. Tseng, W.C. Shen, J.S. Wang, K.J. Chen, M.Y. Cheng, J. Rick, Y.J. Huang, F.C. Chang, B.J. Hwang, J. Mater. Chem. 21 (2011) 10448–10453.
[22] Y.S. Ye, G.W. Liang, B.H. Chen, W.C. Shen, C.Y. Tseng, M.Y. Cheng, J. Rick, Y.J. Huang, F.C. Chang, B.J. Hwang, J. Power Sources 196 (2011) 5408–5415.
[23] H.C. Kolb, M.G. Finn, K.B. Sharpless, Angew. Chem. Int. Ed. 40 (2001) 2004–2021.
[24] R. Huisgen, Angew. Chem. Int. Ed. 7 (1968) 321–328.
[25] V.V. Rostovtsev, L.G. Green, V.V. Fokin, K.B. Sharpless, Angew. Chem. Int. Ed. 41 (2002) 2596–2599.
[26] P. Wu, A.K. Feldman, A.K. Nugent, C.J. Hawker, A. Scheel, B. Voit, J. Pyun, J.M.J. Fréchet, K.B. Sharpless, V.V. Fokin, Angew. Chem. Int. Ed. 43 (2004) 3928–3932.
[27] A.J. Scheel, H. Komber, B.I. Voit, Macromol. Rapid Commun. 25 (2004) 1175–1180.
[28] W. Agut, D. Taton, S. Lecommandoux, Macromolecules 40 (2007) 5653–5661.
[29] E.P. Giannelis, Adv. Mater. 8 (1996) 29–35.
[30] G. Choudalakis, A.D. Gotsis, Eur. Polym. J. 45 (2009) 967–984.
[31] M. Alexandre, P. Dubois, Mater. Sci. Eng. Rep. 28 (2000) 1–63.
[32] Y.S. Ye, Y.C. Yen, C.C. Cheng, Y.J. Syu, Y.J. Huang, F.C. Chang, Polymer 51 (2010) 430–436.
[33] Y.J. Huang, Y.S. Ye, Y.C. Yen, L.D. Tsai, B.J. Hwang, F.C. Chang, Int. J. Hydrogen Energy 36 (2011) 15333–15343.
[34] Y.S. Ye, M.Y. Cheng, J.Y. Tseng, G.W. Liang, J. Rick, Y.J. Huang, F.C. Chang, B.J. Hwang, J. Mater. Chem. 21 (2011) 2723–2732.
[35] Y.F. Lin, C.Y. Yen, C.C.M. Ma, S.H. Liao, C.H. Hung, Y.H. Hsiao, J. Power Sources 165 (2007) 692–700.
[36] T. Watari, H. Wang, K. Kuwahara, K. Tanaka, H. Kita, K.I. Okamoto, J. Membr. Sci. 219 (2003) 137–147.
[37] C.W. Lin, Y.F. Huang, A.M. Kannan, J. Power Sources 164 (2007) 449–456.
[38] Y.S. Ye, Y.C. Yen, W.Y. Chen, C.C. Cheng, F.C. Chang, J. Polym. Sci. A: Polym. Chem. 46 (2008) 6296–6304.
[39] Y.I. Norimitsu Tohnai, M. Miyata, N. Yasui, E. Mochizuki, Y. Kai, Bull. Chem. Soc. Jpn. 72 (1999) 851–858.
[40] W.F. Chen, P.L. Kuo, Macromolecules 40 (2007) 1987–1994.
[41] J. Ding, C. Chuy, S. Holdcroft, Adv. Funct. Mater. 12 (2002) 389–394.

[42] T. Fu, Z. Cui, S. Zhong, Y. Shi, C. Zhao, G. Zhang, K. Shao, H. Na, W. Xing, J. Power Sources 185 (2008) 32–39.
[43] P. Bébin, M. Caravanier, H. Galiano, J. Membr. Sci. 278 (2006) 35–42.
[44] B. Kumar, J.P. Fellner, J. Power Sources 123 (2003) 132–136.
[45] A.A. Kornyshev, A.M. Kuznetsov, E. Spohr, J. Ulstrup, J. Phys. Chem. B 107 (2003) 3351–3366.
[46] A.S. Badami, A. Roy, H.S. Lee, Y. Li, J.E. McGrath, J. Membr. Sci. 328 (2009) 156–164.
[47] R. Gosalawit, S. Chirachanchai, S. Shishatskiy, S.P. Nunes, J. Membr. Sci. 323 (2008) 337–346.
[48] Z. Gaowen, Z. Zhentao, J. Membr. Sci. 261 (2005) 107–113.
[49] T.K. Kim, M. Kang, Y.S. Choi, H.K. Kim, W. Lee, H. Chang, D. Seung, J. Power Sources 165 (2007) 1–8.
[50] J. Won, H.H. Park, Y.J. Kim, S.W. Choi, H.Y. Ha, I.H. Oh, H.S. Kim, Y.S. Kang, K.J. Ihn, Macromolecules 36 (2003) 3228–3234.
[51] R. Herrera Alonso, L. Estevez, H. Lian, A. Kelarakis, E.P. Giannelis, Polymer 50 (2009) 2402–2410.
[52] J. Wang, J. Du, J. Zhu, C.A. Wilkie, Polym. Degrad. Stab. 77 (2002) 249–252.
[53] M. Zanetti, G. Camino, P. Reichert, R. Mülhaupt, Macromol. Rapid Commun. 22 (2001) 176–180.
[54] M. Zanetti, G. Camino, R. Thomann, R. Mülhaupt, Polymer 42 (2001) 4501–4507.